INTERNATIONAL JOURNAL OF Electroactive Materials

Int. J. Electroactive Mater. **5 (2017) 56-61**
www.electroactmater.com

RECEIVED
15 December 2017

REVISED
26 December 2017

ACCEPTED FOR PUBLICATION
29 December 2017

PUBLISHED
30 December 2017

Effect of Alkaline Solution on the Phase Structure and Microstructure of Corroded Sn-3.0Ag-0.5Cu Solder

Nurwahida Mohd Zaini[1], Mukridz Md Mohtar[1], Ahmad Azmin Mohamad[2], Muhammad Firdaus Mohd Nazeri[1,*]

[1]School of Materials Engineering, Universiti Malaysia Perlis, 02600 Jejawi, Kangar, Perlis, Malaysia
[2]School of Materials and Mineral Resources Engineering, Universiti Sains Malaysia, 14300 Nobong Tebal, Penang, Malaysia.
E-mail: firdausnazeri@unimap.edu.my*

ABSTRACT: The use of Sn-3.0Ag-0.5Cu (SAC305) solder on electronic products requires assured reliability information, including corrosion resistant capabilities since the demand for device miniaturization and portability are keep increasing. To achieve this, the corrosion properties of SAC305 were evaluated in 6 M KOH by means of potentiodynamic polarization. To further understand the electrochemical reaction taking place, additional characterizations such as X-ray diffraction and scanning electron microscope analyses were performed. Lowest equilibrium corrosion potential and passivation current were obtained at the scan rate of 1 mV/s. Passivation film was seen at the surface of the solder after polarization, resulted from dissolution of Sn. Phase identification revealed that SnO and SnO2 were the responsible phases for the formation of passivation.
Keywords: Corrosion; SAC; Scan rate; Passivation; Tin oxide.

1. Introduction

The tin-silver-copper (Sn-Ag-Cu) solders are very promising candidates to replace toxic Sn-Pb solders in electronic industry due to its of good solderability, mechanical properties and also low melting temperature [1], especially for near-eutectic Sn-3.0 wt. % Ag-0.5 wt. % Cu (SAC305). To ensure lead-free solders are fully reliable to replace Sn-Pb solders, corrosion resistance aspect needed to be fully addressed. Since modern electronic devices and gadgets are mostly portable, the risk of exposure towards corrosion environment is higher. Worse, miniaturization of electronic devices and gadgets, increasing density of connection on a single electronic circuit and complex structure would worsen the effect of corrosion if corrosion agent is present.

Although electronic circuit was kept in most stringent protection from environment, source of corrosion cannot be completely ignored. For example, presence of thermal cyclic can lead to humidity build-up within the electronic devices or gadgets [2]. Besides that, trace of chemical from etching processes [2] or leakage of electrolyte from batteries [3] might also pose serious corrosion attack. Therefore, more in depth research is needed in order to have a better understanding of the effect of corrosion media in the corrosion of lead free solder.

Various researches have been conducted purposely to study the corrosion behavior of SAC305 solder, especially in 3.5 wt. % sodium chloride (NaCl). SAC305 produced better corrosion resistance compared with Sn-Ag in 3.5 wt. % NaCl due to higher passivation potential and lower passivation current density [4]. Thermal properties of SAC305 were also strictly affected by corrosion. See et al. [5] reported that calculated heat of fusion for SAC305 decreased significantly as corrosion exposure extended. Yet, it was also explained that the gap of the pasty range for this solder and its melting point does not affected by corrosion attack. In term of mechanical properties, the SAC305 behave differently between bulk solder and joint condition under exposure of 3.5 wt. % NaCl. Presence of Cu bonding pad introduces galvanic corrosion between bulk solder and bonding pad. Consequently, this introduces solidification crack on the solder joint [6]. Nevertheless, the studies of corrosion in other corrosion media such as alkaline solution e.g: potassium hydroxide (KOH) is very limited and remains unclear [7]. KOH is one of commonly found alkaline solutions. Several reports show that this alkaline solution capable of inducing severe corrosion attack on solder joints [7]. To ensure SAC305 served reliably in application, corrosion performance of this solder in KOH solution is worthy to be investigated.

In this study, corrosion behaviour between SAC305 solder in 6 M KOH will be presented. Corrosion parameters such as equilibrium corrosion potential (E_{corr}), equilibrium corrosion current (I_{corr}) and passivation current (I_{pass}) of each solder will be investigated at different scan rates. The morphology and phase of the polarized solder will be also be studied to allow better understanding the corrosion process taking place.

2. Experimental

2.1 Sample preparation

Commercially supplied SAC305 (Dagu electronic) was rolled into coil and re-melted at temperature of 300 °C. The molten solder then was cast and air-cooled to room temperature. Then, the alloy was pressed and mechanically punched to produce pellets with diameter of 5 mm and 3 mm thickness. Each solder pellet was attached to a copper (Cu) wire with 1 mm diameter to provide electrical connections. The alloys were cold-mounted with epoxy resin and were ground, polished and cleaned to obtain a mirror finish surface prior to electrochemical analysis.

2.2 Corrosion testing

Potentiodynamic polarization was performed using three-electrode system consist of a platinum plate as counter electrode, mercury-mercury oxide (Hg/HgO) as reference electrode and the SAC305 as the working electrode. A potentiostat (AUTOLAB PGSTAT 30) was used to conduct the corrosion test in 6 M HCl electrolyte. In this study, different scanning rate of 0.5, 1.0, 1.5 and 2.0 mV/s were used, with applied potential range of -2.0 to 2.0 V for all scanning rate. For each scan rate, the electrochemical measurement was repeated for three times to ensure reproducibility of the results. The optimum scan rate was chosen for further in-depth microstructure and phase characterizations.

2.3 Microstructure and phase analysis

Scanning electron microscope (NOVA NANOSEM 450) equipped by energy dispersive spectroscopy (X-Max 50, OXFORD) was used to determine the microstructure and corrosion products compositions of SAC305 solder after corrosion testing. Phase analysis analyzed by using X-Ray Diffractometer (Shimadzu XRD 6000) at 2θ ranging from 20 to 90°. XPERT Highscore Plus software was then used to analyze the results obtained in accordance to International Committee of Diffraction Data (ICDD) X-Ray data files.

3. Results and discussion

3.1 Potentiodynamic polarization

The potentiodynamic polarization profile for SAC305 solder in 6 M KOH solution (**Figure 1**) can be divided into two regions which are cathodic (part1) and anodic regions (part 2-6). The scans begin in the cathodic region at a potential of -2.0 $V_{Hg/HgO}$. As the applied potential increased to -1.12 $V_{Hg/HgO}$, the current decreased rapidly from 0.17 x 10^{-3} A to 0.153 x 10^{-6} A. The reaction involved in cathodic domain is [4, 8, 9]:

$$O_2 + 2H_2O + 4e^- \rightarrow 4OH^- \quad (1)$$

The beginning of anodic region was shown by the increase of current up to 0.0189 A with further increase of applied potential (part 2). This part is known as the primary activation region where the dissolution of Sn is expected. The linear slopes in cathodic and anodic regions signify the equilibrium corrosion potential (E_{corr}) and equilibrium corrosion current density (i_{corr}) of SAC305 solder. As the applied potential increases, hydrogen evolution process were seen (part 3) due to the local collapse of the surface oxide [10]. At the same time, initiation of passivation process at the surface took place. This causes the current value to fluctuate in this region.

As the applied potential increased, passivation process continued. This leads to the formation of passivation layer on the surface, known as the primary passivation region (part 4). Continuous significant decreases in current were seen regardless of the applied potential. In this part, the lowest current of 0.929 x 10^{-2} A was recorded, possibly attributed to the formation of complete passivation film.

Beyond this point, increase of applied potential causes the current to increase steadily (part 5) where passivation film breakdown and its recovery processes occur simultaneously [11]. The last part in polarization scan of SAC305 solder is stated as secondary passivation region (Part 6) where the current was seen to become independent of potential again. This may be contributed by the completion of passivation film recovery process [12].

The potentiodynamic polarization result for solder SAC305 in 6 M KOH solution at different scan rate (**Figure 2**) exhibit almost similar linear cathodic behavior for all scan rates. Value of E_{corr} are observed to be consistent except at scan rate 1.0 mV/s, where it shows the highest value indicates that the solder achieve earlier steady state condition at 1.0 mV/s compared to others and the active region at this scan rate occurs earlier than in others (**Table 1**).

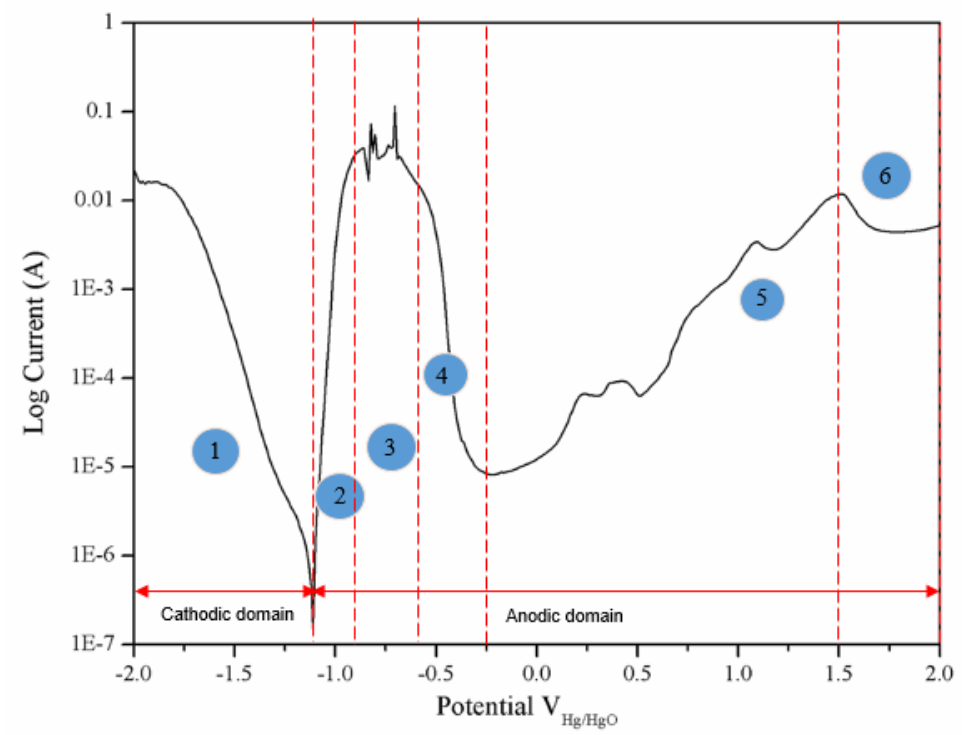

Figure 1: Potentiodynamic polarization of SAC305 solder in 6 M KOH solution at scan rate 1.0 mV/s

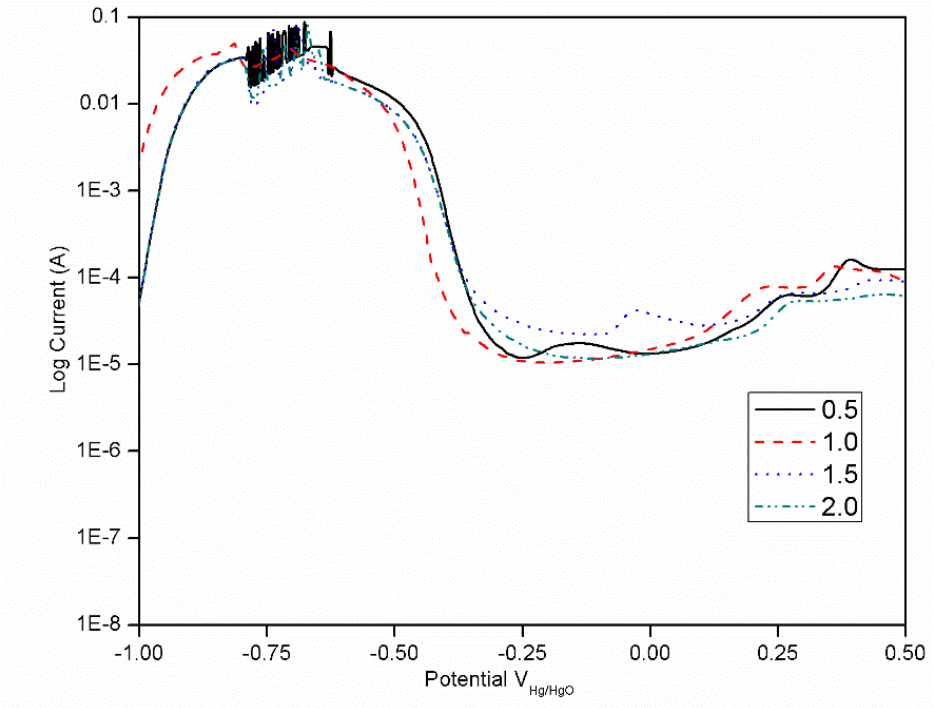

Figure 2: Potentiodynamic polarization curves of SAC305 solder at different scanning rate

Table 1: Electrochemical parameters obtained from polarization curves of SAC305 in 6 M KOH

Scan rate (mV/s)	E_{corr} (v)	I_{corr} (A)	I_p (A)
0.5	-1.072	0.711×10^{-6}	1.38×10^{-5}
1.0	-1.132	1.17×10^{-6}	0.85×10^{-5}
1.5	-1.055	1.53×10^{-6}	2.25×10^{-5}
2.0	-1.077	0.592×10^{-6}	1.19×10^{-5}

3.2 Morphological analysis

The microstructure of as-prepared SAC305 consist of black-crystal, grey-crystal and light grey matrix (**Figure 3a**). The black-crystal represents Cu_6Sn_5, while grey crystal and light grey crystal represents Ag_3Sn and β-Sn phase respectively [14]. The phases of Cu_6Sn_5 and Ag_3Sn are barely visible in the microstructure. According to Rosalbino et.al [15], small solubility of Ag in the Ag_3Sn, Cu in Cu_6Sn_5 and both elements in Sn causes the appearance of Cu_6Sn_5 and Ag_3Sn are very small. Comparable appearance was also reported by Liew et.al [16].

The microstructure of cathodic domain (**Figure 3b**) is observed to be comparable to Figure 3a where the microstructure shows the presence of β-Sn matrix with barely visible phases of Cu_6Sn_5 and Ag_3Sn. As the KOH solution is exposed to atmosphere, thus the solution contains dissolved oxygen. Part 2 represented by the beginning of anodic domain in primary activation region where it involved the dissolution of Sn thus forms groove and pitting at the solder surfaces that can be seen in the microstructure (**Figure 3c**). The electrode potential of Sn was lower than Ag and Cu, thus Sn is considered as the most active metal and acts as an anode in the solder alloy. Therefore, Sn was more easily dissolved compared to Ag and Cu. Tin dissolved through the reaction [4, 16]:

$$Sn \rightarrow Sn^{2+} + 2e^- \quad (2)$$

As the polarization continues the Sn dissolution was hindered by the formation of oxide layer that contributes to the passivation region. The microstructure (**Figure 3d**) shows the formation of loosely-packed oxide layer. The grooves and pitting are partially covered by the formation of oxide layer believed to be SnO from $Sn(OH)_2$ on the solder surface. The reaction involved are [4, 16]:

$$Sn + 2OH^- \rightarrow Sn(OH)_2 + 2e^- \quad (3)$$

$$Sn(OH)_2 \rightarrow SnO + H_2O \quad (4)$$

As the polarization continued, formation of continuous oxide layer is seen (**Figure 3e**). The loosely packed oxide layer barely visible as the passivation process continue and forming more compact oxide layer. This continuous oxide layer offered protection from further dissolution. As a result, the corrosion current was significantly reduced under primary passivation region. The polarization continues and the microstructure (**Figure 3f**) reveal the presence of compact oxide layer with loosely packed oxide layer due to the breakdown of oxide layer in transpassive region. Therefore, revealing part of the solder fresh surface that are no longer protected by the oxide layer. Thus, causing secondary dissolution of Sn occur. However, the dissolution process quickly covered by secondary formation of oxide layer. Both dissolution of Sn and formation of oxide layer continue to occur simultaneously and forming both loosely packed oxide layer with compact oxide layer. This result is consistent with Liew et.al [16] where it ascribed the formation of secondary oxide layer which likely SnO_2 resulted by the formation of SnO and $Sn(OH)_2$ into $Sn(OH)_4$. The microstructure of last part in polarization analysis (**Figure 3g**) shows the formation of fully compact oxide layer which marks the end of potentiodynamic polarization process. The reaction can be described as [4, 16]:

$$SnO + H_2O + 2OH^- \rightarrow Sn(OH)_4 + 2e^- \quad (5)$$

$$Sn(OH)_2 + 2OH^- \rightarrow Sn(OH)_4 + 2e^- \quad (6)$$

$$Sn(OH)_4 \rightarrow SnO_2 + H_2O \quad (7)$$

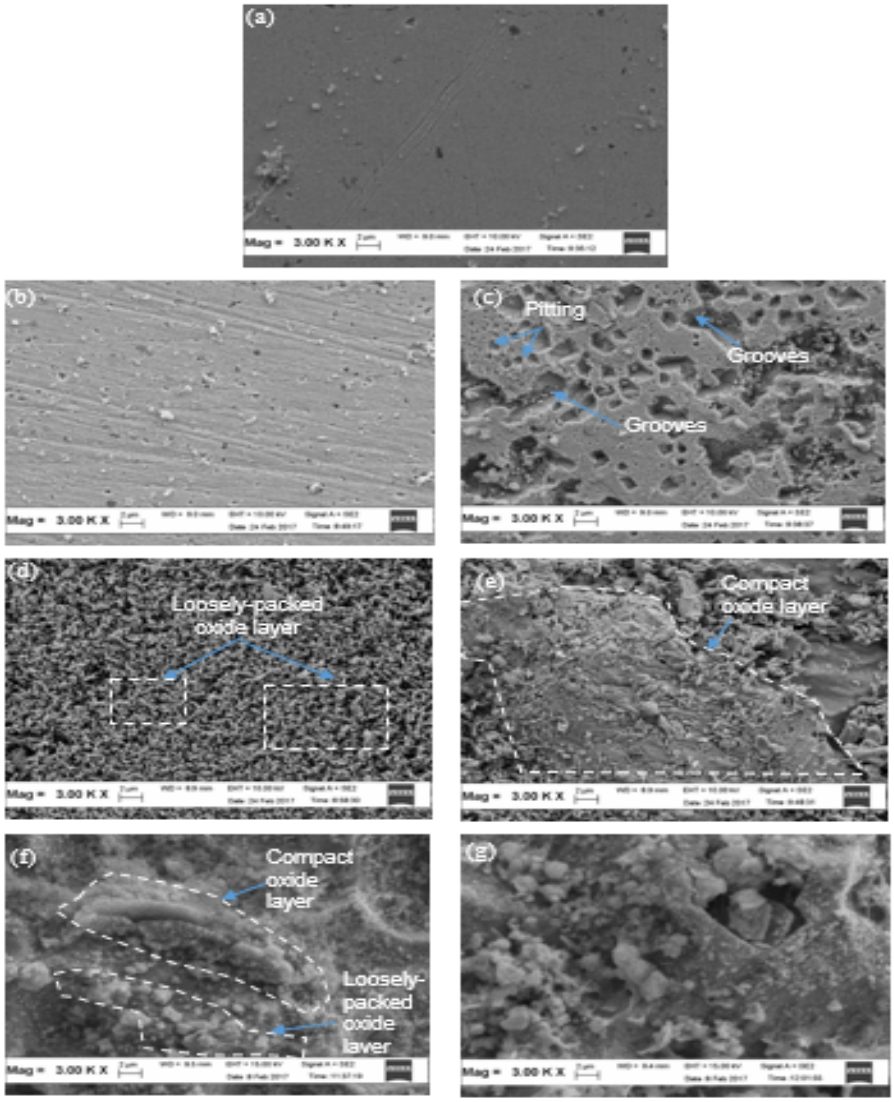

Figure 3: FESEM images for solder SAC305 in 6 M KOH by part: (a) as-prepared, (b) part 1, (c) part 2, (d) part 3, (e) part 4, (f) part 5 and (g) part 6

3.3 Phase analysis

As-prepared SAC305 solder shows presence of β-Sn, Ag_3Sn and Cu_6Sn_5 phase (**Figure 4**). This result verified the finding in section 3.2 where only three different phases were seen. The presence of these three phases are also in accordance with other research [15]. Identical result was also obtained for Part 1 (cathodic region).

New phases of SnO and SnO_2 were evidenced for part 2 and 3. Since Sn was dissolved during primary activation region (part 2), the intensity of peaks for Sn phase was reduced. Furthermore, reaction of Sn ions with hydroxyls produces SnO and SnO_2, exactly as predicted by Equation 3-7. Peak intensities for Ag_3Sn phase were also decreased as the passivation film fully covered the solder surface in part 4, to achieve primary passivation stage.

In part 5 and part 6, SnO and SnO_2 phases were becoming more dominant. Yet, detection of Cu_6Sn_5 and Ag_3Sn are apparent. Passive film breakdown due to high potential applied seen in the potentiodynamic polarization profile in this region might play major role in revealing both of these phases [10]. Passive film breakdown allows fresh solder surface underneath the passivation film to be expose. Consequently, this allows the rise of current detected due to Sn dissolution, while simultaneously revealing the Cu_6Sn_5 and Ag_3Sn.

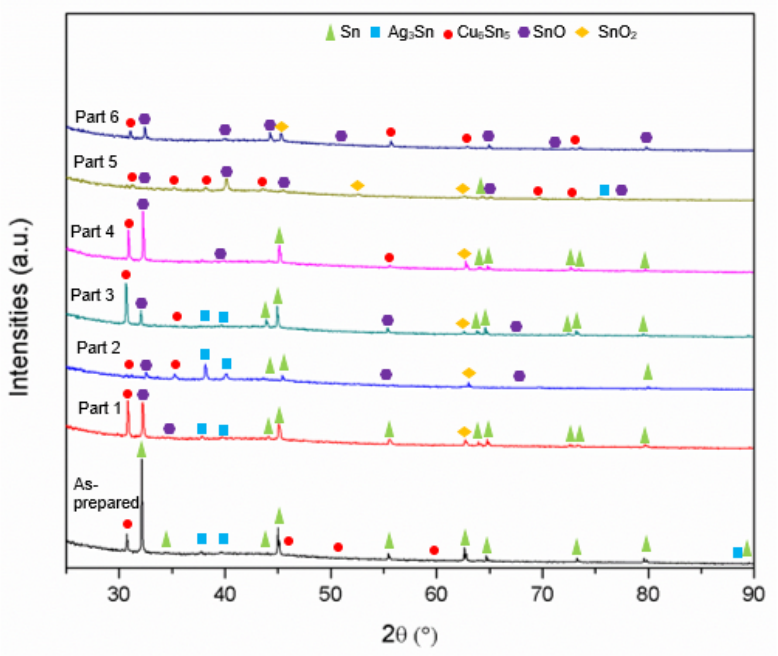

Figure 4: XRD pattern for solder SAC305 in 6 M KOH solution at scan rate 1.0 mV/s

4. Conclusions

Corrosion behavior of SAC305 in 6 M KOH was investigated by means of potentiodynamic polarization. It was found that scan rate of 1 mV/s allows the solder to achieve earlier steady state condition, while requiring the lowest current to generate oxide thickening. Phase analysis revealed that SnO and SnO2 were produced due to dissolution of Sn. Presence of these corrosion products also responsible to the formation of passivation layer, as proven by microstructure analysis.

Acknowledgement

The authors would like to acknowledge the financial support from UniMAP Short term Grant (9001-00548).

References

1. S. Martin, M. Drienovsky, T. Lydia, P. Marian, Metal 2015, Czech Republic, EU.
2. V. Chidambaram, J. Hald, R. Ambat, and J. Hattel, JOM-J Min. Met. Mat. S., 61 (2009) 59-65.
3. B. Kennedy, D. Patterson, S. Camilleri, J. Power Sources, 90 (2000) 156-162.
4. D. Li, P. P. Conway, C. Liu, Corros. Sci., 50 (2008) 995-1004.
5. C. W. See, M. Z. Yahaya, H. Haliman, A. A. Mohamad, Procedia Chem., 19 (2016) 847-854.
6. M. Wang, J. Wang, W. Ke. Microelectron. Reliab., 73 (2017) 69-75.
7. M. F. Mohd Nazeri and A. A. Mohamad, J. Alloy. Compd., 661 (2016) 516-525.
8. K. Kim, S. Huh, and K. Suganuma, Microelectron. Reliab., 43 (2003) 259-267.
9. W. R. Osorio, L. C. Peixoto, L. R. Garcia, A. Garcia, and J. E. Spinelli, Inter. J. Electrochem. Sci., 7 (2012) 6436.
10. M. F. M. Nazeri, A. B. Ismail, and A. A. Mohamad, J. Alloy. Compd., 606 (2014) 278-287.
11. J.-C. Liu, S. Park, S. Nagao, M. Nogi, H. Koga, J.-S. Ma, et al., Corros. Sci., 92 (2015) 263-271.
12. J.-C. Liu, G. Zhang, S. Nagao, J.-T. Jiu, M. Nogi, T. Sugahara, et al. Corr. Sc., 99 (2015) 154-163.
13. M. Curioni and F. Scenini, Electrochim. Acta, 180 (2015)712-721.
14. F. Rosalbino, E. Angelini, G. Zanicchi, R. Carlini, and R. Marazza, Electrochimi. Acta, 54 (2009) 7231-7235.
15. F. Rosalbino, E. Angelini, G. Zanicchi, and R. Marazza, Mater. Chem. Phys., 109 (2008) 386-391.
16. M. C. Liew, I. Ahmad, L. M. Lee, M. F. M. Nazeri, H. Haliman, and A. A. Mohamad, Metall. Mater. Trans. A, 43 (2012) 3742-3747.